Nuclear Instruments and Methods in Physics Research A ▮ (▮▮▮▮) ▮▮▮–▮▮▮

Contents lists available at ScienceDirect

Nuclear Instruments and Methods in Physics Research A

journal homepage: www.elsevier.com/locate/nima

The MEG timing counter calibration and performance

M. De Gerone [a,b], S. Dussoni [a,b], K. Fratini [a,b], F. Gatti [a,b], R. Valle [a,b], G. Boca [c,d], P.W. Cattaneo [c], M. Rossella [c], R. Nardó [c,d], A. Papa [e], G. Signorelli [f,g], G. Cavoto [h], G. Piredda [h,*], F. Renga [h,i], C. Voena [h], Y. Uchiyama [j]

[a] INFN Sez. di Genova, via Dodecaneso 33, Genova, Italy
[b] Dip. di Fisica dell'Universitá, via Dodecaneso 33, Genova, Italy
[c] INFN Sez. di Pavia, via A. Bassi 6, Pavia, Italy
[d] Dip. di Fisica Nucleare e Teorica, via A. Bassi 6, Pavia, Italy
[e] Paul Scherrer Institut, 5232 Villigen, Switzerland
[f] INFN Sez. di Pisa, L.go B.Pontecorvo 2, Pisa, Italy
[g] Dip. di Fisica, L.go B.Pontecorvo 2, Pisa, Italy
[h] INFN Sez. di Roma, P.le A.Moro 2, Roma, Italy
[i] Dip. di Fisica, Universitá Sapienza, P.le A.Moro 2, Roma, Italy
[j] ICEPP, University of Tokyo, 7-3-1 Hongo, Bunkyo-ku, Tokyo 113-0033, Japan

ARTICLE INFO

Article history:
Received 5 October 2010
Received in revised form
22 December 2010
Accepted 12 February 2011

Keywords:
Time resolution
Calibration
Neutrinoless muon decay

ABSTRACT

The MEG experiment has been taking data at the Paul Scherrer Institute (Switzerland) since 2008 to search for the rare decay $\mu^+ \to e^+\gamma$. In order to reduce the huge accidental background, it is crucial to reach a high resolution on the e^+ time measurement through a dedicated Timing Counter detector. We report the methods for calibrating and the performance achieved by the Timing Counter in the early phase of the experiment.

1. Introduction

The goal of the MEG experiment [1] is to search for the lepton flavor violating decay $\mu^+ \to e^+\gamma$ with a sensitivity of 10^{-13} in the branching ratio, improving the current best limit [2] by two orders of magnitude. For a muon at rest, the $\mu^+ \to e^+\gamma$ decay has a clear two-body final state topology in which the decay positron and γ-ray are emitted simultaneously and back-to-back, each with an energy of 52.8 MeV, corresponding to half of the muon mass. Positive muons are used to avoid the formation of muonic atoms and muon capture on the target nuclei. The background is dominated by the accidental coincidence of a positron originating from the normal Michel decay of the muon and a γ-ray originating from other sources, e.g. radiative muon decay ($\mu^+ \to e^+ \nu_e \bar{\nu}_\mu \gamma$) or annihilation-in-flight of another Michel positron. In order to identify $\mu^+ \to e^+\gamma$ events out of a huge background a precise measurement of the energy, relative emission angle and time of positron and γ-ray is mandatory.

The MEG apparatus (see Figs. 1 and 2) is located at the Paul Scherrer Institut (PSI) in Switzerland. Three key elements enable the excellent sensitivity of the experiment: (*i*) a high rate continuous muon beam, (*ii*) an innovative liquid Xenon (LXe) scintillation γ-ray detector [4], and (*iii*) a specially designed positron spectrometer [5] with a gradient magnetic field (0.4–1.2 T) and a scintillation timing counter array for fast timing and triggering.

The Timing Counter (TC) [6] consists of two sectors (upstream and downstream of the target) each one made of 15 BC404 plastic scintillating bars with approximately square cross-section ($4 \times 4\ \mathrm{cm}^2$) and equal length (80 cm), placed parallel to the z-axis, around a circumference with a radius of about 30 cm from the target. We adopt a coordinate reference system with the z-axis along the beam direction, y is the vertical axis and ϕ is the angle in the (x, y) plane. The TC ϕ coverage is between -140° and 10° to intercept the positrons emitted back-to-back with respect to the photons in the LXe acceptance. Downstream (upstream) bars are labeled from 0 to 14 (from 15 to 29) with bar 0 (15) located at the highest ϕ value. Each bar is read-out at either end by a fine-mesh Hamamatsu 2″ photomultiplier tube (PMT) able to withstand the spectrometer magnetic field. A set of 256,

* Corresponding author.
E-mail address: giancarlo.piredda@roma1.infn.it (G. Piredda).

0168-9002/$ - see front matter © 2011 Elsevier B.V. All rights reserved.
doi:10.1016/j.nima.2011.02.044

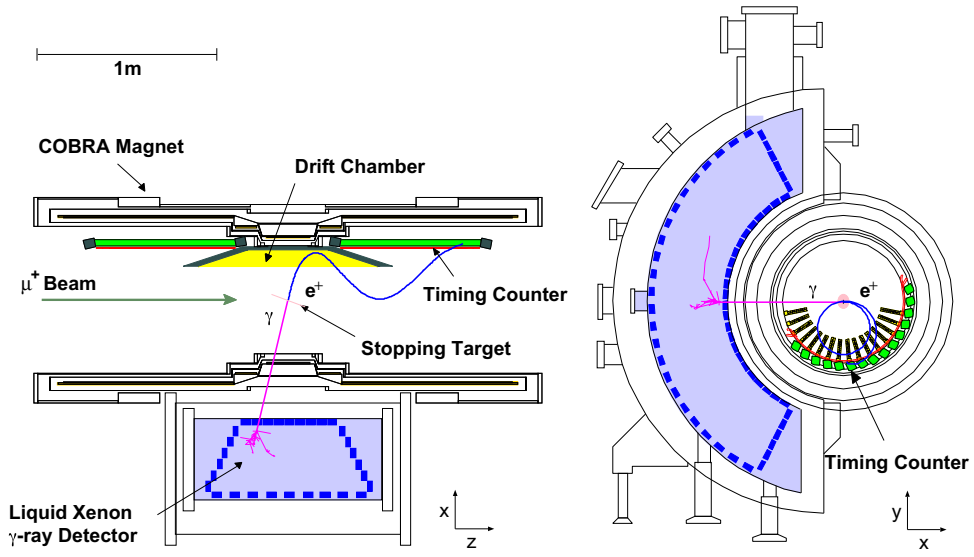

Fig. 1. The MEG detector: left, top view; right, front view.

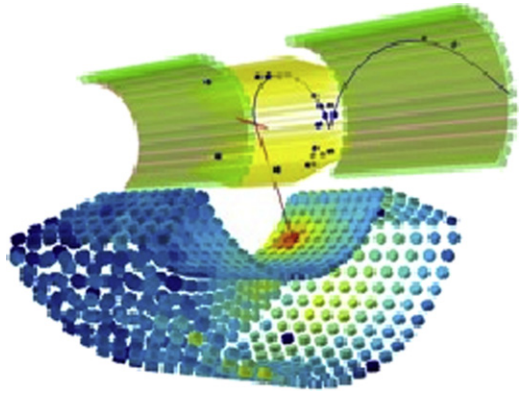

Fig. 2. Pictorial view of a 'signal-like' event acquired by the MEG detector. Top: a positron tracked in the spectrometer hits two bars in the TC. Bottom: schematic of the energy released by the photon in the Liquid Xenon Calorimeter.

$5 \times 5\ \mathrm{mm}^2$ square scintillating fibers is assembled in the transverse direction in each sector to improve the measurement the z-coordinate of the positron impact point and for triggering on particles within the detector acceptance. However, because of unforeseen integration problems, the performance of this component is not reported here.

The TC detector is designed to measure, at the level of a few tens of picosecond, the time at which the positron impinges on the scintillating bars. This can be done by averaging the measurements of the time provided by the two PMTs positioned at each end of the bars. The difference of these two measurements can be related to the z-coordinate of the positron impact point. As it will be discussed in this paper, the PMT time measurements have constant relative offsets, due to the electronic chain, which must be determined in order to have a uniform response of the detector. Moreover, since the time measurement is realized with a constant voltage threshold discriminator, a *time-walk* effect is generated, and this must be taken into account to optimize the resolution. We describe below the calibration procedures for the timing and the z-coordinate measurements determined from the analysis of the signal from the scintillating bars. This paper is organized as follows. Section 2 introduces the basic relation between the measured quantities and the positron impact time at the TC. Section 3 includes all the calibrations, while the conclusions and the performances are reported in Section 4.

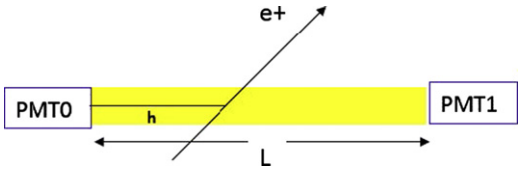

Fig. 3. Sketch of a TC scintillating bar crossed by a positron. Inner PMT0 (outer PMT1) yields a t_0 (t_1) time measurement, respectively.

2. TC timing basics

The times measured by the two TC PMTs, t_0 and t_1 for the inner and outer (with respect to the target) PMT respectively (see Fig. 3), can be written as:

$$t_0 = T + \frac{c_0}{\sqrt{A_0}} + \frac{h}{v_{\mathrm{eff}}} + b_0 \tag{1}$$

$$t_1 = T + \frac{c_1}{\sqrt{A_1}} + \frac{L-h}{v_{\mathrm{eff}}} + b_1 \tag{2}$$

where T is the time of arrival of the positron at the timing counter bar, measured with respect to an arbitrary reference, the terms $c_i/\sqrt{A_i}$ represent the time-walk correction (see Section 3.1 and e.g. Ref. [3]), the A_i are the PMT pulse heights, h is the distance of the impact point from the inner PMT, L is the bar length, v_{eff} is the effective scintillation light velocity and the b_i represent any electronic time offsets. The effective velocity is assumed here to be constant along the bar and to be the same for all the bars. This has been verified to be true to an approximation good enough for the purpose of the present work.

The PMT times t_0 and t_1 are determined off-line from fits to the NIM output pulses of the double threshold discriminators (DTD), which are digitized by the custom designed 'Domino Ring Sample' DRS3 [7] (see Fig. 4).

Typical DTD thresholds are 25 and 800 mV for low and high threshold respectively. The arrival time T of the positron at the TC is derived by adding Eqs. (1) and (2) above

$$T = \frac{t_0+t_1}{2} - \frac{1}{2}\left(\frac{c_0}{\sqrt{A_0}} + \frac{c_1}{\sqrt{A_1}}\right) - \left(\frac{L}{2v_{\mathrm{eff}}} + \frac{b_0+b_1}{2}\right) \tag{3}$$

Please cite this article as: M. De Gerone, et al., Nucl. Instr. and Meth. A (2011), doi:10.1016/j.nima.2011.02.044

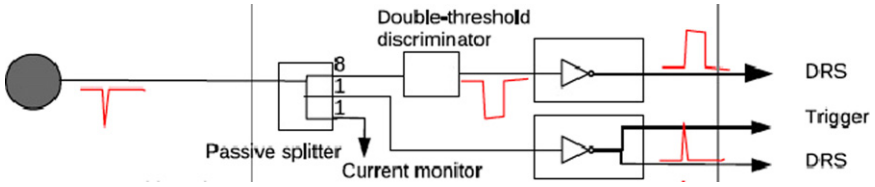

Fig. 4. Scheme of the TC PMT signal read-out chain.

Table 1
Calibration constants and corresponding data sample utilized for their extraction.

Kind of calibration	Constant	Data sample
Time-walk correction	c_k	Michel
Offset between PMTs same bar	b_0-b_1	cosmic
Offset between bars	b_0+b_1	boron and Dalitz

and similarly by subtraction the value of h is found

$$h = v_{\text{eff}}\left[\frac{t_0-t_1}{2}-\frac{1}{2}\left(\frac{c_0}{\sqrt{A_0}}-\frac{c_1}{\sqrt{A_1}}\right)+\left(\frac{L}{2v_{\text{eff}}}-\frac{b_0-b_1}{2}\right)\right]. \quad (4)$$

Note that the term (b_0+b_1) in Eq. (3) is a *constant* characteristic of each bar and is assumed to be the *inter-bar time offset*, while the term (b_0-b_1) in Eq. (4) enters in the determination of h, and will discussed later. Both quantities T and h can be obtained once the calibration constants v_{eff}, b_k, and c_k are determined. We note that in measuring the arrival time, there are quantities which fluctuate event by event (A_k) and constant biases that depend on the hardware properties or electronic readout chains. Correcting for the former improves the *single* bar time resolution while accounting for the latter allows us to equalize the response of *all* the scintillating bars when the TC time must be compared to the LXe calorimeter time measurement. In Table 1 we summarize the calibration constants and the data samples used for their extraction. To conclude this section, we remark that the c_k are the coefficients for the time-walk correction, and therefore they are needed for the optimization of the time resolution, whereas the b_k parameters enter either in the difference (b_0-b_1), to correct the unbalance between time delays for the z determination along the same bar, or in the sum (b_0+b_1), when the time offset between bars has to be found.

3. The timing counter calibrations

After a rough equalization of the PMTs high voltage, the time-walk correction is applied. Then the time alignment of the PMTs of the same bar is addressed and finally all the bars are synchronized with respect to the LXe PMTs.

The first step consists of the charge equalization of the PMTs. This is achieved using cosmic rays hitting the center of each bar. The HV of each PMT is then tuned so that the pulse height difference is within 30% at both ends of each bar and the total energy read-out is almost constant for all the bars.

3.1. The time-walk correction

The time is determined by the intercept of a fixed threshold with the NIM signal generated by the DTD. The *time-walk* effect, which needs correction in order not to spoil the time resolution, originates from the correlation between the time measurement and the signal pulse height because of the use of a fixed voltage threshold, as shown in Fig. 5. To correct that effect we adopt the

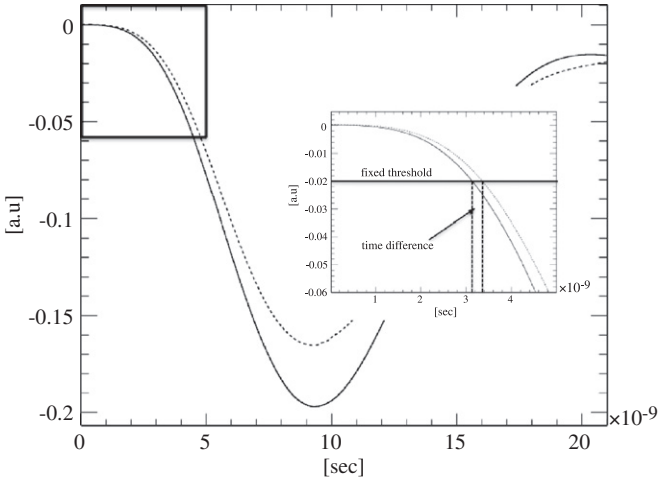

Fig. 5. The time-walk effect. Due to a fixed threshold, two simultaneous signals but with different pulse heights give different time determinations, as shown in the inset.

Fig. 6. A positron crossing three adjacent bars, each providing a time measurement T_X.

following procedure. We define as *double* (*triple*) events those with one and only one cluster of two (three) adjacent hit bars.

In a sample of *triple* events it is possible to extract from data the calibration constants b_k and c_k. Given three bars B, A and C where B is the first hit bar by the positron, A the second (central) and C the third (see Fig. 6), with very good approximation:

$$T_A = \frac{T_B+T_C}{2} \quad (5)$$

and

$$h_A = \frac{h_B+h_C}{2}. \quad (6)$$

Using Eqs. (1) and (2) for the measured times t and assuming an equal effective velocity in all the bars we can write

$$t_{kA} = \frac{t_{kB}-f_{kB}(A_{kB})+t_{kC}-f_{kC}(A_{kC})}{2}+f_{kA}(A_{kA}) \quad (7)$$

where $f_{kX}(A_{kX}) = b_{kX}+c_{kX}(1/\sqrt{A_{kX}})$, $k=0, 1$ for the inner and outer PMT respectively, and $X=A, B, C$ is the bar index. We notice that in deriving Eq. (6) the h_X distances cancel out.

By a least squares method, we extract simultaneously the parameters b_k and c_k for all the bars and for all PMTs by

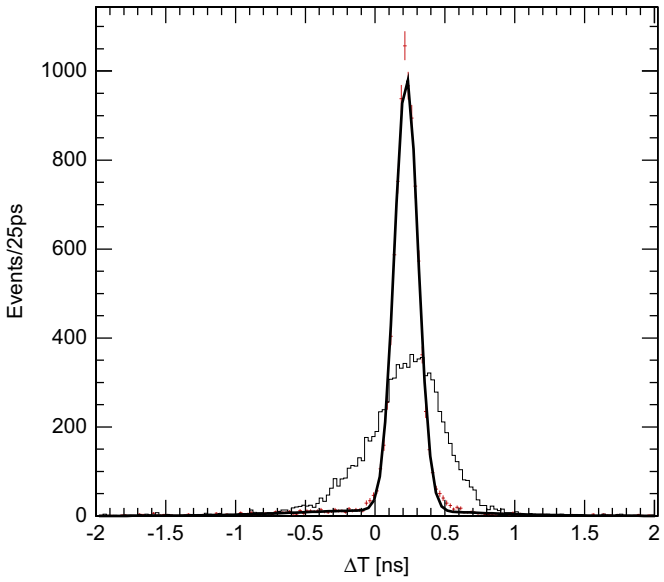

Fig. 7. ΔT_{raw} (light) and ΔT (dark) distribution in double events (for bar 2) with a double Gaussian fit. The improvement due to the time-walk correction is clearly visible. The left tail is due to pathological events with hits from secondary processes.

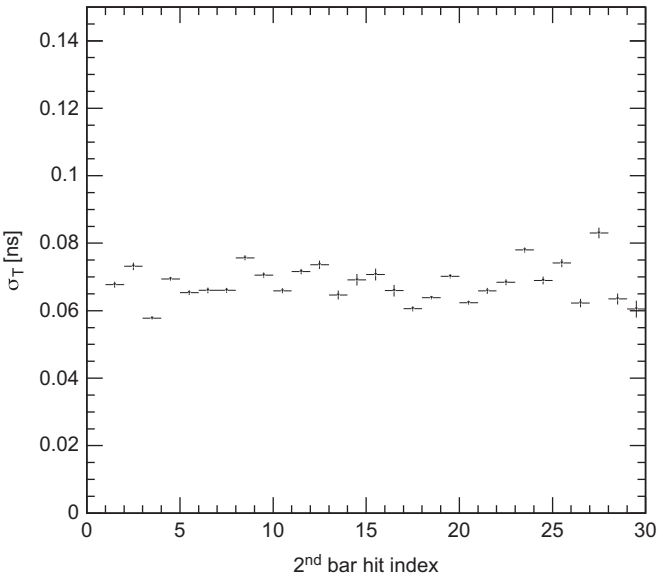

Fig. 8. Summary of $\sigma(\Delta T)/\sqrt{2}$ from double Gaussian fits for all the bars (doubles sample) in Michel data.

minimizing, in turn for each $k=0$, 1, the quantity

$$\Sigma_{j=0}^{N}\left(\left[t_{kA}^{j}-\frac{t_{kB}^{j}+t_{kC}^{j}}{2}\right]-\left[f_{kA}(A_{kA}^{j})-\frac{f_{kB}(A_{kB}^{j})+f_{kC}(A_{kC}^{j})}{2}\right]\right)^{2} \tag{8}$$

where N is the number of *triple* events.

The c_k coefficients turn out to have similar values (about 0.4 ns $V^{1/2}$) whereas this method yields only a poor determination of the b_k parameters. The b_k offsets will be, therefore, found by a different approach as reported below.

Having derived the parameters from the *triple* sample, we apply the time-walk correction ($c(1/\sqrt{A})$) to the PMTs in an independent sample of *double* events as a cross-check. Let A and B be any two adjacent bars, we evaluate first the time-walk uncorrected time difference

$$\Delta T_{raw}=\frac{t_{0A}+t_{1A}}{2}-\frac{t_{0B}+t_{1B}}{2} \tag{9}$$

where t_{kA} (t_{kB}) are the times measured by the PMTs on the second (first) hit bar and the index 0(1) stands for the inner (outer) PMT, respectively.

We then apply the time-walk correction by evaluating for each pair of bars:

$$\Delta T=\Delta T_{raw}-\left(\frac{c_{0A}\frac{1}{\sqrt{A_{0A}}}+c_{1A}\frac{1}{\sqrt{A_{1A}}}}{2}-\frac{c_{0B}\frac{1}{\sqrt{A_{0B}}}+c_{1B}\frac{1}{\sqrt{A_{1B}}}}{2}\right). \tag{10}$$

We fit the distributions of this variable for each *double* event with a double Gaussian function, extracting the mean value and the standard deviation σ of the core component (see Fig. 7 for an example of such a fit). Since the two bars provide uncorrelated time measurements, the value of $\sigma/\sqrt{2}$ can be interpreted as the time resolution (σ_T) of each bar or, better, as an upper limit to the TC intrinsic time resolution. The implicit assumption that the first and the second bar hit have equal time resolution is not strictly correct because the interactions of the positron as it passes through the first bar spoil the accuracy of the time measured by the PMTs of the second bar. In Fig. 8 we show the resolutions for all the bars and this represents the final result for the TC intrinsic time resolution. The following sections are devoted to the time alignment of the PMTs of the same bar (or z-measurement calibration) and to the inter-bar synchronization.

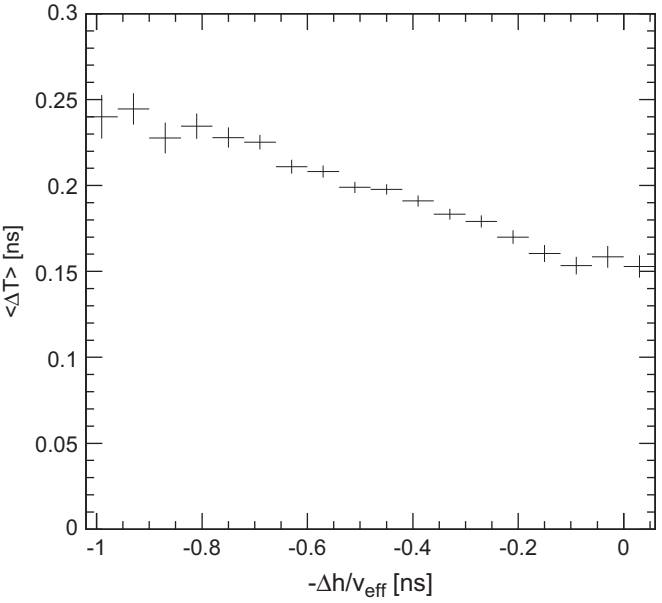

Fig. 9. Mean value (in ns) of ΔT distribution in double events vs the difference $-\Delta h$. A clear correlation is visible: a larger $|\Delta h|$ corresponds to a larger mean value of ΔT.

We notice that the resolutions are in a range between 60 and 70 ps when the core Gaussian of the full distribution is considered. The distributions, however, present left tails (see Fig. 7) due to events in which there are hits out of the positron track and due to secondary processes. Moreover, there is another reason for which the quoted resolutions represent an upper limit on the TC intrinsic time resolution. The ΔT distribution is actually the superposition of several distributions with narrower widths and different mean values. Such a mean value depends on the incidence angle of the positron to the bars. We show this effect in Fig. 9 where the mean value of ΔT is correlated with the difference (Δh) of the h measured by the two bars. For larger $|\Delta h|$ we see larger ΔT mean values.

Please cite this article as: M. De Gerone, et al., Nucl. Instr. and Meth. A (2011), doi:10.1016/j.nima.2011.02.044

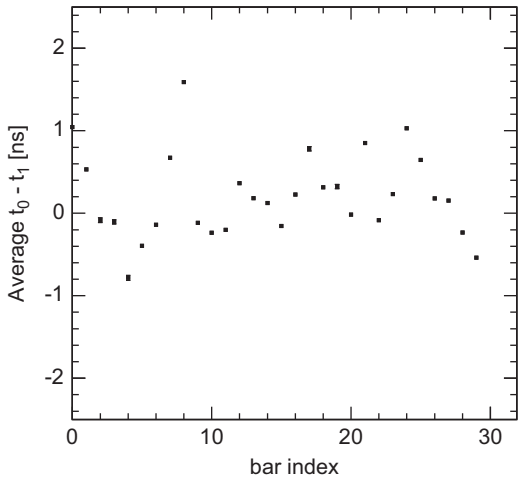

Fig. 10. Mean values of the time-walk corrected time difference distribution for cosmics events for each bar.

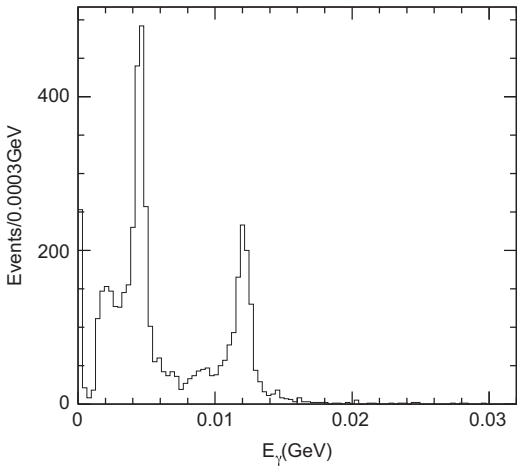

Fig. 11. Photon energy distribution reconstructed by the LXe calorimeter in boron events. The 4.4 and 11.7 MeV peaks are clearly visible.

3.2. Time alignment between PMTs of the same bar

As already shown in Section 2 the determination of the difference (b_0-b_1) is necessary in order to adjust correctly the z-measurements for each bar.

The longitudinal position h (z-coordinate) of the impact point of the positron on the bar can be determined if the effective velocity v_{eff} is known (see Fig. 3). More explicitly the mean value of

$$h+\frac{L}{2}-\frac{v_{\text{eff}}}{2}(b_0-b_1)=\frac{v_{\text{eff}}}{2}\left[(t_0-t_1)-\left(c_0\frac{1}{\sqrt{A_0}}-c_1\frac{1}{\sqrt{A_1}}\right)\right] \tag{11}$$

averaged over the h interval between 0 and L, represents a characteristic constant of each bar (*inter PMT offset*) and must be determined from data.

This has been done using a sample of cosmic events for which the distribution of the impact point should be flat along the bar. The mean value of the time-walk corrected time difference $[(t_0-t_1)-(c_0(1/\sqrt{A_0})-c_1(1/\sqrt{A_1}))]$ distribution gives the inter PMT offset.

In Fig. 10 we show the offsets derived from a large sample of cosmic events. We checked their stability by iterating the procedure periodically. We note that for some bars the offset determination is not satisfactory – the z-distribution being not exactly flat – which is probably due to an insufficient gain equalization between the two PMTs of the bars concerned. Furthermore, on beam data, we observe a small asymmetry in the number of bars hit in the downstream sector (bar number <15) with respect to the upstream. This has been interpreted as due to muons decaying downstream of the target. The hit distribution as a function of the bar number (i.e. ϕ of positron impact point) is not flat due to the unequal presence of material along the path of the positron, in good agreement with the MC simulation.

3.3. Inter-bar offset calibration

The synchronization among all the bars is achieved by detecting two simultaneous photons in the LXe calorimeter and in the TC, where one bar at a time is hit. This is realized by means of an auxiliary 1 MeV Cockcroft–Walton (C–W) [9] accelerator mainly operated for the LXe calibrations. The reaction $^{11}\text{B}(p,\gamma)^{12}\text{C}$ is excited by protons impinging on a lithium tetraborate target. Two photons emerge from this reaction simultaneously and almost isotropically, with energy of 4.4 MeV (low energy photon) and 11.7 MeV (high energy photon) as shown in Fig. 11. We were able to take advantage of the frequent (two or three times per week) C–W data taking already planned for the LXe calibrations.

We require the energy of the photon in the LXe to be less than 8 MeV, selecting those events in which the low energy photon enters the calorimeter and the high energy photon hits the TC. We consider $T_{\gamma\gamma}$, the time difference of the two photons from the boron reaction, measured by the LXe calorimeter and the TC, computed at the target by subtracting the photons times of flight:

$$T_{\gamma\gamma}=\left(T_{\gamma,LXe}-\frac{L_{\gamma,LXe}}{c}\right)-\left(T_{\gamma,TC}-\frac{L_{\gamma,TC}}{c}\right) \tag{12}$$

where $T_{\gamma,LXe}$ is the time measured by the LXe [8] and $L_{\gamma,LXe}/c$ is the photon time of flight from the origin of the apparatus to the calorimeter, $T_{\gamma,TC}$ is the TC time of the first hit bar, using the algorithm described above, $L_{\gamma,TC}/c$ is the photon time of flight from the origin to the TC, and c is the speed of the light. We assume that the C–W target is point-like and correctly located at the center of the apparatus, corresponding to the origin of the coordinate reference system. The impact point at the TC has the TC (fixed) radius and the z measured from the time difference of the PMTs measurement.

The time $T_{\gamma,LXe}$ is already corrected at this stage for the time offsets between different calorimeter PMTs. Thus, since the two photons are emitted simultaneously, for photons impinging on the bar j of the TC we can write

$$T_{\gamma\gamma,j}=\frac{L}{2v_{\text{eff,j}}}+\frac{b_{0,j}+b_{1,j}}{2}+T_{\text{off}}=k_j+T_{\text{off}} \tag{13}$$

where T_{off} is time offset between LXe and TC, because the two times in the sub-detectors are measured with respect to independent clocks. In Fig. 12 the $T_{\gamma\gamma,j}$ distribution for a reference bar (bar # 17) is shown. We fit the distribution, for each bar j, to a Gaussian function, in a range of 1.2 ns around its maximum. The mean value of the Gaussian is the offset k_j+T_{off}. We stress here that the we are interested in comparing the averages of the distributions, related to the time offsets we are looking for, rather than their widths, which depend on the time resolution. Incidentally, the time resolution in these events is worse than in μ-beam data due to the poor time of flight determination (lack of vertex determination as the intersection of the reconstructed positron track with the target plane) and the different photon statistics in the TC scintillator. We arbitrarily assume bar 17 as a reference and define the interbar-offset of the j-th bar the quantity k_j-k_{17}. The tails of the distribution are due to cosmic rays, as we have verified by taking data with the C–W accelerator switched off. The systematic effect due to the cosmic ray background is negligible

Please cite this article as: M. De Gerone, et al., Nucl. Instr. and Meth. A (2011), doi:10.1016/j.nima.2011.02.044

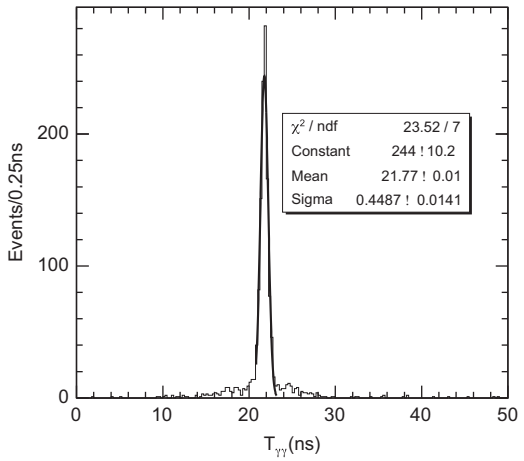

Fig. 12. $T_{\gamma\gamma}$ distribution for a single bar (bar 17) with the Gaussian fit superimposed for boron events.

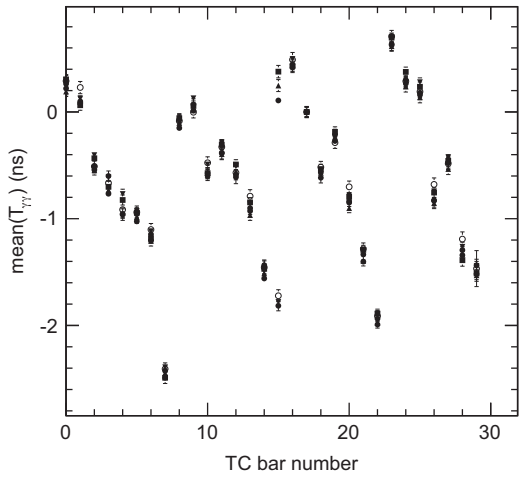

Fig. 13. Inter-bar offsets (relative to bar 17) vs the TC bar number for different periods (typically one week) corresponding to different markers.

for almost all the bars except for the last two less shielded bars on both TC sections, where the maximum contribution turns out to be of the order of 100 ps. Additional systematic effects related to the fitting procedure have been evaluated and found negligible.

We checked the stability of the inter-bar time offsets, which turned out to be acceptable. This can be seen in Fig. 13 where the inter-bar offsets are shown, as a function of the bar number, for various run periods.

3.4. LXe-TC timing validation using π^0 Dalitz decays

As a control sample of the LXe-TC time calibration we use π^0 Dalitz decays ($\pi^0 \to e^+e^-\gamma$) produced in special runs where a liquid hydrogen target was exposed to a π^- beam to yield π^0 through a charge exchange process $\pi^- p \to \pi^0 n$.

These are the only events with a topology very similar to that of the signal, namely with a positron and a photon in the final state (the electron is not reconstructed in the spectrometer). However, due to the extended target, these events are reconstructed with less accuracy and therefore only the average values of the distributions are relevant. We select events with one reconstructed photon in the calorimeter and one reconstructed track matched with a hit in the TC . We consider the quantity $T_{e\gamma}$, the difference of

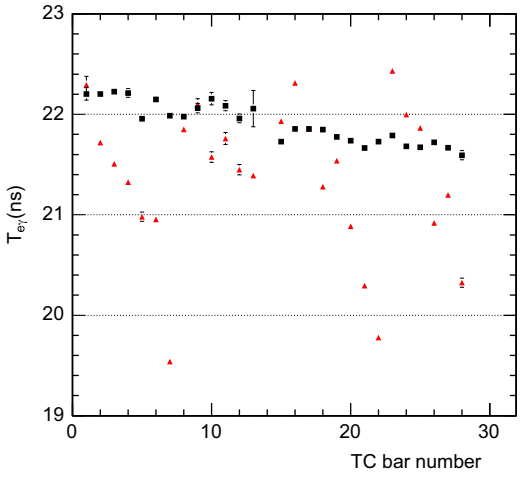

Fig. 14. Inter-bar offsets vs TC bar number on Dalitz data before (triangles) and after (squares) boron calibration. Fit instabilities due to low statistics cause large errors in a few bars.

the time of the photon and of the positron at the target

$$T_{e\gamma} = T_\gamma - \frac{L_\gamma}{c} - T_e + \frac{L_e}{c} \tag{14}$$

very similar to Eq. (13) above, once the γ impinging the TC is replaced by the positron. It is interesting to see how well the boron calibration aligns the TC bars: this can be seen in Fig. 14 where the inter-bar offsets (relative to bar 17) are shown before and after calibration. It is clear that the calibration corrects the bulk of the inter-bar differences but is not perfect, with residual differences among bars up to 400 ps in the downstream part of the detector.

One possible problem is the difference in the energies of the boron and Dalitz sample, as previously noted, the algorithm for time calibration has been performed at an energy much higher than the boron data energy, so a residual time-walk effect can be present. A further irreducible component comes from positrons produced in photon conversions on the liquid hydrogen thin aluminum vacuum chamber, with a $\sim 1\%$ probability competitive to the π^0 Dalitz decay.

4. Conclusions

The calibration procedures described in this paper have been successfully applied to the data taken during year 2008 and the intrinsic TC time resolution is close to the design value of about 45 ps. The use of boron data allowed us to inter-connect the time measurements of all the TC bars, as the double coincidence method cannot be used across the two sectors, and improves the resolution of the relative timing between the LXe and the TC. The resolution on such timing evaluated on a sample of reconstructed radiative muon decays has been shown to be about 150 ps [10], a large improvement with respect to previous experiments searching for $\mu^+ \to e^+\gamma$.

References

[1] A. Baldini, et al., MEG Collaboration, Research Proposal to PSI R-99-05, 1999.
[2] M.L. Brooks, et al., Mega Collaboration, Phys. Rev. Lett. 83 (1999) 1521.
[3] A.W.B. Atwood, Time of flight measurements, SLAC-PUB-2620, October 1980.
[4] T. Iwamoto, the MEG Collaboration, Nucl. Phys. B Proc. Suppl. 172 (2007) 224.
[5] H. Hildebrandt, TIPP Tsukuba Conference, Nucl. Instr. and Meth. A 623 (2010) 111–113.
[6] S. Dussoni, et al., Nucl. Instr. and Meth. A 617 (2010) 387.
[7] S. Ritt, Nucl. Instr. and Meth. A 518 (2004) 470.
[8] Y. Uchiyama, Nucl. Instr. and Meth. A 617 (2010) 118.
[9] MEG Collaboration, Use of a Cockcroft–Walton accelerator for calibrating and monitoring the MEG experiment submitted to NIM.
[10] J. Adam, et al., MEG Collaboration, Nucl. Phys. B 834 (2010) 1.

Please cite this article as: M. De Gerone, et al., Nucl. Instr. and Meth. A (2011), doi:10.1016/j.nima.2011.02.044